U.S. Department
of Transportation
Federal Railroad
Administration

Office of Research,
Development and Technology
Washington, DC 20590

Quick Calibration of Fracture Behaviors in TC128 Steel for Finite Element Modeling

DOT/FRA/ORD-20/46

Final Report | November 2020

NOTICE

This document is disseminated under the sponsorship of the Department of Transportation in the interest of information exchange. The United States Government assumes no liability for its contents or use thereof. Any opinions, findings and conclusions, or recommendations expressed in this material do not necessarily reflect the views or policies of the United States Government, nor does mention of trade names, commercial products, or organizations imply endorsement by the United States Government. The United States Government assumes no liability for the content or use of the material contained in this document.

NOTICE

The United States Government does not endorse products or manufacturers. Trade or manufacturers' names appear herein solely because they are considered essential to the objective of this report.

REPORT DOCUMENTATION PAGE

Form Approved
OMB No. 0704-0188

1. REPORT DATE *(DD-MM-YYYY)*	2. REPORT TYPE	3. DATES COVERED *(From - To)*
November 2020	Technical Report	April 5, 2019 – August 20, 2020

4. TITLE AND SUBTITLE

Quick Calibration of Fracture Behaviors in TC128 Steel for Finite Element Modeling

5a. CONTRACT NUMBER

5b. GRANT NUMBER

5c. PROGRAM ELEMENT NUMBER

6. AUTHOR(S)

Shaun Eshraghi (0000-0002-8152-0838)

Michael Carolan (0000-0002-8758-5739)

5d. PROJECT NUMBER
RR28A400

5e. TASK NUMBER
SB929

5f. WORK UNIT NUMBER

7. PERFORMING ORGANIZATION NAME(S) AND ADDRESS(ES)

Volpe National Transportation Systems Center
55 Broadway
Cambridge, MA 02142

8. PERFORMING ORGANIZATION REPORT NUMBER

9. SPONSORING/MONITORING AGENCY NAME(S) AND ADDRESS(ES)

U.S. Department of Transportation
Federal Railroad Administration
Office of Railroad Policy and Development
Office of Research, Development and Technology
Washington, DC 20590

10. SPONSOR/MONITOR'S ACRONYM(S)

11. SPONSOR/MONITOR'S REPORT NUMBER(S)
DOT/FRA/ORD-20/46

12. DISTRIBUTION/AVAILABILITY STATEMENT

This document is available to the public through the FRA website.

13. SUPPLEMENTARY NOTES

COR: Francisco, González, III

14. ABSTRACT

From April 5, 2019, to August 20, 2020, the Volpe National Transportation Systems Center (Volpe) performed a series of finite element (FE) analyses of uniaxial tensile tests to calibrate material models for tank car steels (TC128) from two recent side impact tests. The material models, which characterize plasticity and ductile fracture, are used in full-scale FE analyses to predict puncture of various tank car designs. This report describes the use of the Bao-Wierzbicki quick calibration procedure to model TC128 fracture. A comparison took place of material models calibrated using test results from dogbone and smooth round bar tensile geometries. Based on the FE analysis results, researchers made recommendations for quick calibration of fracture in TC128.

15. SUBJECT TERMS

Steel fracture, TC128, impact test, DOT-105 tank car, DOT-111 tank car, tank car performance, transportation safety, finite element analysis, finite element, FE, hazardous materials, rolling stock

16. SECURITY CLASSIFICATION OF:			17. LIMITATION OF ABSTRACT	18. NUMBER OF PAGES	19a. NAME OF RESPONSIBLE PERSON
a. REPORT	b. ABSTRACT	c. THIS PAGE		43	Francisco, González, III
					19b. TELEPHONE NUMBER *(Include area code)* (202) 493-6076

Standard Form 298 (Rev. 8/98)
Prescribed by ANSI Std. Z39.18

METRIC/ENGLISH CONVERSION FACTORS

ENGLISH TO METRIC	METRIC TO ENGLISH
LENGTH (APPROXIMATE)	**LENGTH (APPROXIMATE)**
1 inch (in) = 2.5 centimeters (cm)	1 millimeter (mm) = 0.04 inch (in)
1 foot (ft) = 30 centimeters (cm)	1 centimeter (cm) = 0.4 inch (in)
1 yard (yd) = 0.9 meter (m)	1 meter (m) = 3.3 feet (ft)
1 mile (mi) = 1.6 kilometers (km)	1 meter (m) = 1.1 yards (yd)
	1 kilometer (km) = 0.6 mile (mi)
AREA (APPROXIMATE)	**AREA (APPROXIMATE)**
1 square inch (sq in, in^2) = 6.5 square centimeters (cm^2)	1 square centimeter (cm^2) = 0.16 square inch (sq in, in^2)
1 square foot (sq ft, ft^2) = 0.09 square meter (m^2)	1 square meter (m^2) = 1.2 square yards (sq yd, yd^2)
1 square yard (sq yd, yd^2) = 0.8 square meter (m^2)	1 square kilometer (km^2) = 0.4 square mile (sq mi, mi^2)
1 square mile (sq mi, mi^2) = 2.6 square kilometers (km^2)	10,000 square meters (m^2) = 1 hectare (ha) = 2.5 acres
1 acre = 0.4 hectare (he) = 4,000 square meters (m^2)	
MASS - WEIGHT (APPROXIMATE)	**MASS - WEIGHT (APPROXIMATE)**
1 ounce (oz) = 28 grams (gm)	1 gram (gm) = 0.036 ounce (oz)
1 pound (lb) = 0.45 kilogram (kg)	1 kilogram (kg) = 2.2 pounds (lb)
1 short ton = 2,000 pounds (lb) = 0.9 tonne (t)	1 tonne (t) = 1,000 kilograms (kg) = 1.1 short tons
VOLUME (APPROXIMATE)	**VOLUME (APPROXIMATE)**
1 teaspoon (tsp) = 5 milliliters (ml)	1 milliliter (ml) = 0.03 fluid ounce (fl oz)
1 tablespoon (tbsp) = 15 milliliters (ml)	1 liter (l) = 2.1 pints (pt)
1 fluid ounce (fl oz) = 30 milliliters (ml)	1 liter (l) = 1.06 quarts (qt)
1 cup (c) = 0.24 liter (l)	1 liter (l) = 0.26 gallon (gal)
1 pint (pt) = 0.47 liter (l)	
1 quart (qt) = 0.96 liter (l)	
1 gallon (gal) = 3.8 liters (l)	
1 cubic foot (cu ft, ft^3) = 0.03 cubic meter (m^3)	1 cubic meter (m^3) = 36 cubic feet (cu ft, ft^3)
1 cubic yard (cu yd, yd^3) = 0.76 cubic meter (m^3)	1 cubic meter (m^3) = 1.3 cubic yards (cu yd, yd^3)
TEMPERATURE (EXACT)	**TEMPERATURE (EXACT)**
[(x-32)(5/9)] °F = y °C	[(9/5) y + 32] °C = x °F

QUICK INCH - CENTIMETER LENGTH CONVERSION

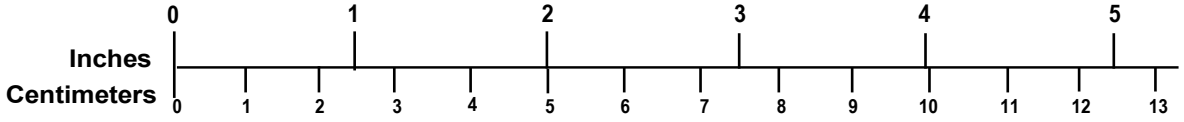

QUICK FAHRENHEIT - CELSIUS TEMPERATURE CONVERSIO

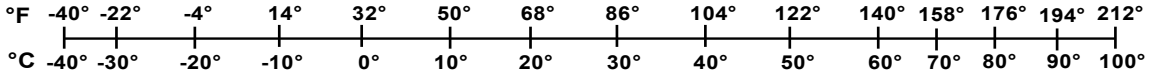

For more exact and or other conversion factors, see NIST Miscellaneous Publication 286, Units of Weights and Measures. Price $2.50 SD Catalog No. C13 10286

Updated 6/17/98

Acknowledgements

The authors would like to thank Francisco González, III, of the Federal Railroad Administration, Benjamin Perlman, and David Jeong (retired) of the Volpe National Transportation Systems Center (Volpe) for their contributions to the tank car shell impact research program. The authors would also like to thank former Volpe employee Joshua Leung for compiling publicly available tensile test data on Association of American Railroads TC128, Grade B steel.

The authors would also like to acknowledge Transportation Technology Center, Inc. for performing the shell impact tests and contracting test labs for tensile testing.

Contents

Illustrations

Tables

Equations

Executive Summary

The tests and analyses described in this report support the overall objective of a Federal Railroad Administration (FRA) research program to improve transportation safety for tank cars. From April 5, 2019, to August 20, 2020, the Volpe National Transportation Systems Center (Volpe) analyzed the fracture of steel (TC128) used in the construction of tank cars designed to carry hazardous materials using finite element (FE) analyses.

The test results and analyses presented in this report are part of a large research program aimed at developing performance-based testing requirements to evaluate the crashworthiness and structural integrity of tank car designs under a shell (side) impact scenario. Transportation Technology Center, Inc. (TTCI) and Volpe collaborate to conduct shell impact tests of tank car designs and to analyze the results. TTCI conducts the shell impact tests and Volpe performs both pre-test and post-test FE analyses of the impact response to evaluate and improve modeling techniques for tank car puncture involving fluid-structure interaction and material failure.

For a typical shell impact test, TTCI contracts with material testing labs to conduct tensile testing on samples from the shell of the tested tank car. Volpe uses the tensile test results to develop material inputs needed to model material failure in the full-scale FE analysis of the shell impact test. The methodology described in this report for calibrating a fracture locus, used to model the failure of steel, is called the Bao-Wierzbicki (B-W) quick calibration procedure. The B-W quick calibration procedure can use tensile test data from either rectangular dogbone (DB) or smooth round bar (SRB) specimen geometries to create the fracture locus.

This report compares and contrasts the use of either DB or SRB tensile geometries to create a fracture locus using the B-W quick calibration procedure. It was found that fracture loci calibrated using SRB test data were better at predicting TC128 fracture, i.e., elongation at break (EB). Even though SRB specimens require more machining and are unable to be meshed with uniform brick elements in a FE model, the more accurate prediction of EB make SRB specimens preferable for B-W quick calibration of Association of American Railroads TC128, Grade B steel in FE analyses of shell impact tests.

1. Introduction

This report describes research being conducted to understand plasticity and fracture in railroad tank car steel, namely the Association of American Railroads (AAR) TC128, Grade B steel.[1] A summary is presented of material properties on TC128 from two tank cars using various tensile geometries. A methodology is proposed to use the measured tensile properties to create material inputs necessary to model steel plasticity in finite element (FE) analysis. A discussion of the results from calibrating fracture models using various standardized tensile test geometries led to recommendations.

1.1 Background

In the past decade, significant research has been conducted to analyze and improve the impact behavior and puncture resistance of railroad tank cars used to transport hazardous materials. Ultimately, the results of this research program will be used by government regulatory agencies in the United States and Canada (i.e., Federal Railroad Administration [FRA] and Transport Canada [TC], respectively) to establish performance-based requirements and to develop methods to evaluate the crashworthiness and structural integrity of different tank car designs when subjected to a standardized, repeatable shell (side) impact scenario[2] (see Figure 1).

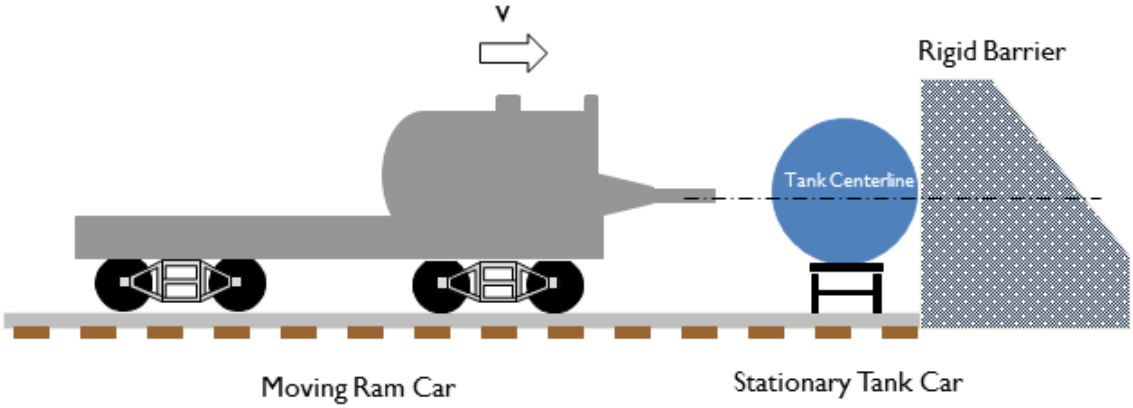

Figure 1. Schematic of Standardized Shell Impact Scenario

Table 1 summarizes the tank car shell impact tests. These shell impact tests have involved testing of tank cars constructed to various specifications, and included a mix of cars designed to carry pressurized gases (DOT-105) and flammable liquids (DOT-111 and DOT-117). Some of these tests were performed as a part of a government-industry collaborative program referred to as the Next Generation Railroad Tank Car Project (denoted with a †).

[1] Association of American Railroads. AAR Specifications for Tank Cars, Appendix M. M-1002. 2019.
[2] Transportation Technology Center, Inc. "Test Implementation Plan for FRA Tank Car Side Impact, Revision 1." April 14, 2016.

Table 1. Summary of Tank Car Shell Impact Tests

Test #	Test Date *MM/DD/YYYY*	Specification	Impact Speed *mph*	Impactor Size *inches*	Reference
1	4/26/2007	DOT-105†	14.0	17 x 23	[1]
2	7/11/2007	DOT-105†	15.1	6 x 6	[1]
3	5/18/2011	DOT-105 (w/ panel)	17.8	12 x 12	[2]
4	5/18/2013	DOT-111	14.0	12 x 12	[3]
5	2/26/2014	DOT-112	14.7	12 x 12	[4]
6	4/27/2016	DOT-105	15.2	12 x 12	[5]
7	9/28/2016	DOT-117	13.9	12 x 12	[6]
8	8/1/2018	DOT-105	9.7	6 x 6	[7]
9	10/30/2018	DOT-111 (CPC-1232)	13.9	12 x 12	[8]

Figure 2 shows a still frame, taken just prior to puncture, from a high-speed camera during a 2018 test of a DOT-105 tank car (see Test 8 in Table 1). To make the test repeatable, controllable, and safe, the tank car is removed from its trucks (bogies) and placed on two skids that limit the roll of the tank car. The tank car is centered perpendicularly on a set of railroad tracks against a stiff impact wall. A ram car weighing approximately 297,000 pounds is equipped with an impact head which can vary in size and accelerated by gravity along track with a slight descending grade resulting in a controllable initial kinetic energy.

Figure 2. Still Frame from Shell Impact Test in 2018 of DOT-105 Tank Car (Test 8)

Because of difficult-to-control variables in the side impact testing, such as impact speed, unknown weld qualities, and the inherent variability of material behavior even within a single plate, there is no such thing as a certain test outcome. In an ideal test, the target test speed would be chosen to fall somewhere in the shaded range in Figure 3, where puncture is possible, but not certain.

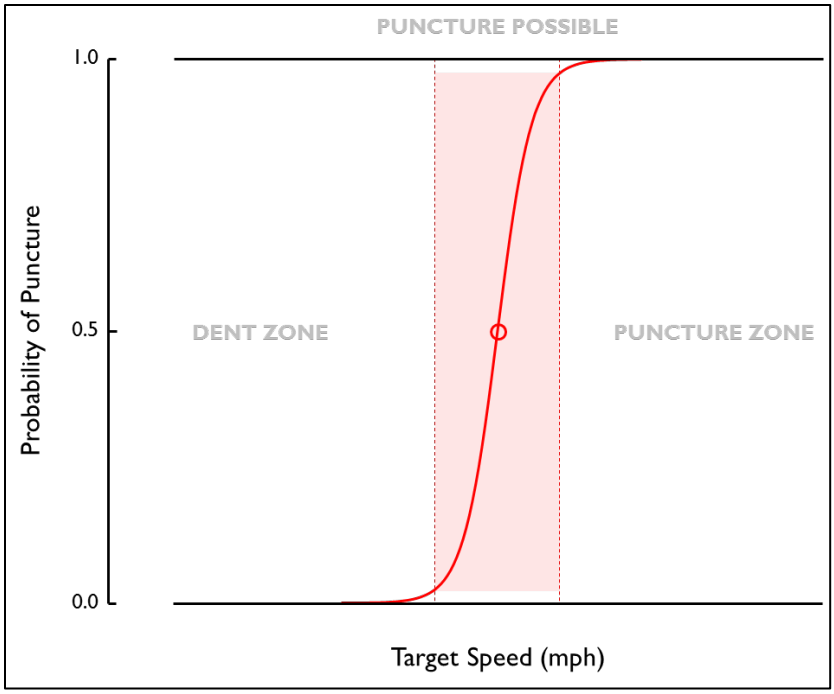

Figure 3. Schematic Illustrating Probability of Puncture vs. Impact Speed

The value of a test can be increased by targeting an impact speed that is very close to the threshold speed between where the tank car punctures and where it does not puncture for a given impactor shape, size, and mass. If the tested impact speed is close to this threshold speed, regardless of whether or not the tank punctures, the data that is collected can be extremely valuable for quantifying the energy-absorption capacity of the tank car for the tested outage and pressure. As the test speed moves further from the center of the puncture threshold range, the value of the test data decreases.

The FE analysis was used to model the shell impact tests and determine the target impact speed prior to each test. The FE analysis has been conducted to examine the puncture behavior of the railroad tank under the generalized shell impact scenario for all the tests in Table 1. Furthermore, when the finite element model is validated by accurately describing the response of the tank car to the tested impact condition, then other studies can be conducted using the same model to investigate other impact conditions which can be useful for understanding the puncture resistance of the tank car in accident conditions and developing performance requirements in future rulemakings.

This report focuses on the material behavior of TC128 steel, which is widely used in the construction of tank cars containing hazardous materials. Specifically, this report examines several approaches to characterizing TC128 steel through laboratory tests, and generating input data that describes the TC128 properties for use in puncture simulations. While it is a conservative engineering practice to assume minimum material properties when making design calculations, a tank car with a shell made from TC128 that only barely meets the minimum mechanical properties (see Table 2) may have a much lower ability to resist puncture than a tank car with "typical" modern TC128 or TC128 that greatly exceeds the norm. When validating a model of a tank car against impact tests data, it is important that the material behaviors used in

the FE model represent the actual behavior of the particular TC128 steel in the tested tank car to allow for a fair comparison to be made between tested car and modeled car.

Table 2. Minimum Properties for TC128

Property	Value
Yield Strength	50,000 psi
Ultimate Tensile Strength	81,000 psi
Elongation at Failure	22% (2-inch gauge)
Elongation at Failure	16% (8-inch gauge)

1.2 Objectives

The objectives of this research are to: (1) summarize tensile testing data on TC128, and (2) present lessons learned when calibrating material properties including plastic behavior and ductile failure for TC128 steel for use in FE models.

1.3 Overall Approach

FRA has conducted a series of shell impact tests on various tank car designs. The Volpe National Transportation Systems Center (Volpe) created pre-test FE models used during test planning to determine the impact speed. After the test, Volpe validates the FE model using the actual test conditions and steel (TC128) properties. The validated FE model can then be used to analyze the performance of the tank car under different accident conditions to inform crashworthiness requirements.

This report focuses on the calibration of TC128 material models used as inputs in the pre- and post-test FE models of the shell impact test. The FE models of the shell impact test require accurate representation of the plastic hardening and ductile fracture behavior of TC128. The report presents a straightforward calibration procedure which can create such a material input. This calibration procedure requires only a single set of test results from standardized uniaxial tensile tests that are widely available from test labs.

1.4 Scope

This report includes a discussion of developing and executing some of the FE models used in the tank car research program, namely modeling tensile tests of TC128. The research presents tensile test results, discusses the execution of the tensile tests, and summarizes the overall results of the tests. Additionally, the authors provided the equations and processes used to adapt tensile test measurements into input data for specific FE software that describes the plasticity and fracture responses of TC128 steel samples.

While this report refers to previously-performed shell impact tests on different tank cars, there is no mention of a comparison of results from different tests within the scope of this report. While the TC128 material models developed using the techniques and tensile test results described in this research is implemented into simulations of full-scale shell impact tests, the results of those shell impact simulations are absent in this report. Research into the puncture resistance of tank cars is ongoing, and further advancements in plasticity and fracture modeling will likely be considered in future work.

1.5 Organization of the Report

Section 1 introduces the work performed and briefly discusses the results obtained.

Section 2 describes the approach taken to characterize ductile fracture in TC128 steels including a description of the Bao-Wierzbicki (B-W) fracture criterion and the B-W quick calibration approach.

Section 3 details the procedure used for calibrating a material model of TC128 from standardized tensile tests and presents tensile test results with corresponding FE analysis results for comparison.

Section 4 includes a summary of the report and contains concluding remarks.

Appendix A offers more information regarding the American Society for Testing and Materials (ASTM) E8 tensile test results.

2. FE Modeling of Ductile Fracture

The material input behaviors for TC128 steel have specifically been developed for use in the Abaqus/Explicit FE software.[3] Abaqus/Explicit is a commercially-available, general purpose explicit FE solver. Volpe used this software throughout the FRA-sponsored tank car puncture modeling program because of its ability to support several modeling techniques required to accurately represent the behavior observed in the different tank car tests. Those modeling techniques include non-linear material behavior for steels, material failure and fracture behaviors, general contact, and the ability to model the liquid (innage) and pressurized gas (outage) within each tank car.

The focus of this report is on the development of material input behaviors that describe TC128 steel. In the modeling approach that Volpe has typically used for tank car impact simulations, there are four material "keywords" in the Abaqus software that are used to describe the properties of TC128 steel. Table 3 summarizes the keywords along with the units used in the FE models.

Table 3. Keywords Used to Describe TC128 Behaviors in FE Models

Keyword	Units	Description
**Density*	*lbf·s²/in⁴*	Defines a material density in terms of mass per unit volume
**Elastic*	*lbf/in²*	Defines a linear elastic modulus in terms of force per unit area
**Plastic, Hardening=Isotropic*	*[lbf/in², N/A]*	Defines isotropic plastic hardening in terms of true stress and plastic equivalent strain $(\bar{\varepsilon}^{pl})$
**Damage Initiation, Criterion=Ductile*	*[N/A,N/A]*	Defines a fracture locus for ductile metals in terms of $(\bar{\varepsilon}^{pl})$ and stress triaxiality (η)
**Damage Evolution, Type=Energy*	*in·lbf/in²*	Defines an energy-based damage progression controlling element stiffness degradation and eventual element removal in terms of fracture energy per unit area

Figure 4 shows an exemplar nominal stress-strain output from an FE model of a tensile coupon with annotations showing regions affected by the various material keywords presented in Table 3. From this diagram, it is clear that the **Elastic* keyword affects only a small portion of the total nominal stress-strain response. The **Plastic* keyword determines a majority of the nominal stress-strain response of the coupon and therefore greatly affects the fracture toughness, i.e., area under the curve. **Damage Initiation* acts as a trigger when elements reach a threshold $\bar{\varepsilon}^{pl}$ value for a given stress state (η). After damage is triggered, **Damage Evolution* determines the rate at which the stiffness of a given element is degraded until its stiffness reaches zero and the element is removed from the simulation. Fracture is completed once all the elements across a cross-

[3] Abaqus 2017. Dassault Systemes Simulia Corp, Providence, RI. 2017.

section of the coupon are removed; at that point (elongation at break) the nominal stress returns to zero.

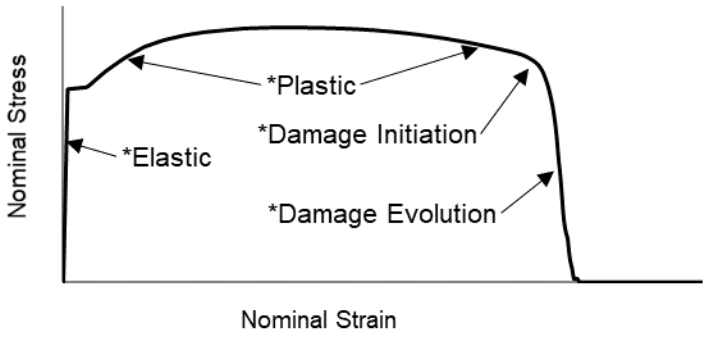

Figure 4. Exemplar Nominal Stress-Strain Output from FE Model with Annotations Showing Regions Affected by Material Keywords

This report describes the material inputs, i.e., keywords, in terms of format for Abaqus/Explicit, but analogous material inputs have been developed [1] for other commercial explicit FE software including LS-DYNA,[4] and with the same overall approach. Density, elastic, and plastic material properties can be specified in LS-DYNA in a material keyword such as **MAT_PIECWISE_LINEAR_PLASTICITY (024)*. Damage initiation and evolution can be specified in a material damage keyword such as **MAT_ADD_DAMAGE_DIEM* or **MAT_ADD_DAMAGE_GISSMO*.

The following two sections focus on the development of a curve (fracture locus) for damage initiation. Section 2.1 describes the fracture locus characterized by an equation called the B-W fracture criterion [9]. Section 2.2 summarizes a simplified calibration procedure for determining the constants in the B-W equation called the B-W quick calibration procedure [10] [11].

2.1 B-W Fracture Criterion

The development of damage and failure by fracture strongly depends on the local state of stress. Stress triaxiality (η) is a parameter that characterizes the local state of stress, and has been recognized as a critical parameter in the ductile fracture of materials. Equation 1 defines triaxiality as the ratio of the hydrostatic stress (σ_H) divided by the von Mises stress (σ_v).

$$\eta = \frac{\sigma_H}{\sigma_v}$$

Equation 1. Stress Triaxiality

Experimental data obtained using round notched round bars (NRB) showed that the effective plastic strain to fracture ($\bar{\varepsilon}_D^{pl}$) decreases monotonically with increasing triaxiality [12] [13] [14]. This trend is consistent with the ductile fracture model developed by Gurson (1977), and later refined by Tvergaard (1981). However, recent experimental evidence demonstrated that for ductile alloys the plastic equivalent strain at fracture is not monotonically related to stress

[4] LS-DYNA Keyword User's Manual, Volume II Material Models, LS-DYNA R11, Livermore Software and Technology Corporation (LSTC), Livermore, CA. 2018.

triaxiality [9] [17] [18] [19] [20] [21]. Figure 5 schematically shows the difference between these various criteria in terms of plastic equivalent strain $(\bar{\varepsilon}^{pl})$ and stress triaxiality.

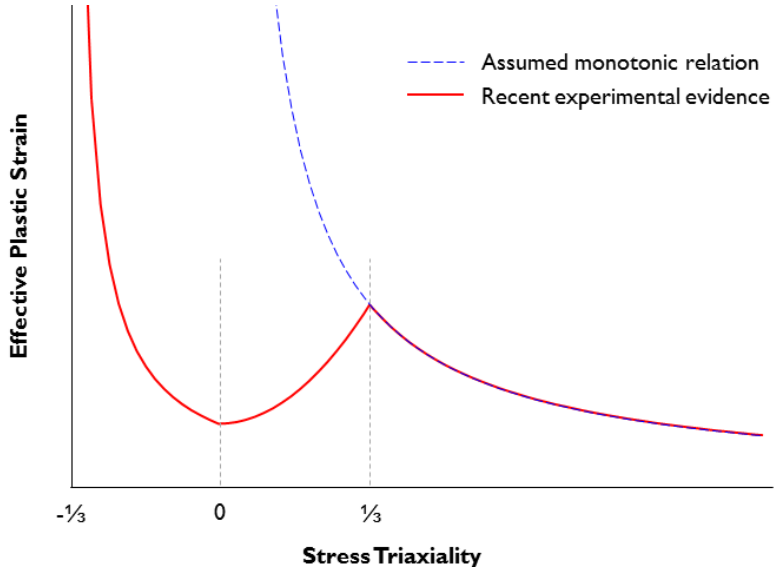

Figure 5. Schematic Comparison of Ductile Fracture Criteria

In the tank car shell impact puncture FE models, a fracture criterion as a function of plastic equivalent strain and stress triaxiality referred to as the B-W criterion was applied [9]. The complete B-W fracture locus for a ductile metal (i.e., TC128) can be calibrated through a series of mechanical tests on 11 unique specimen geometries intended to cover a wide range of stress triaxialities.

Figure 6 shows a schematic of the B-W fracture locus which consists of three regions: I – Ductile Fracture, II – Mixed Fracture, and III – Shear Fracture. When $\eta < 0$ the element is in a state of compression, and when $\eta > 0$ the element is in a state of tension. A triaxiality of $\eta = -1/3$ corresponds to a stress state of hydrostatic compression and $\eta = 0$ corresponds to pure shear. The cusp of the B-W fracture locus is located at the average triaxiality on the fracture surface of a smooth round bar (SRB) specimen under uniaxial tension at $\eta = x_0$ and is typically close to a value of 0.4.

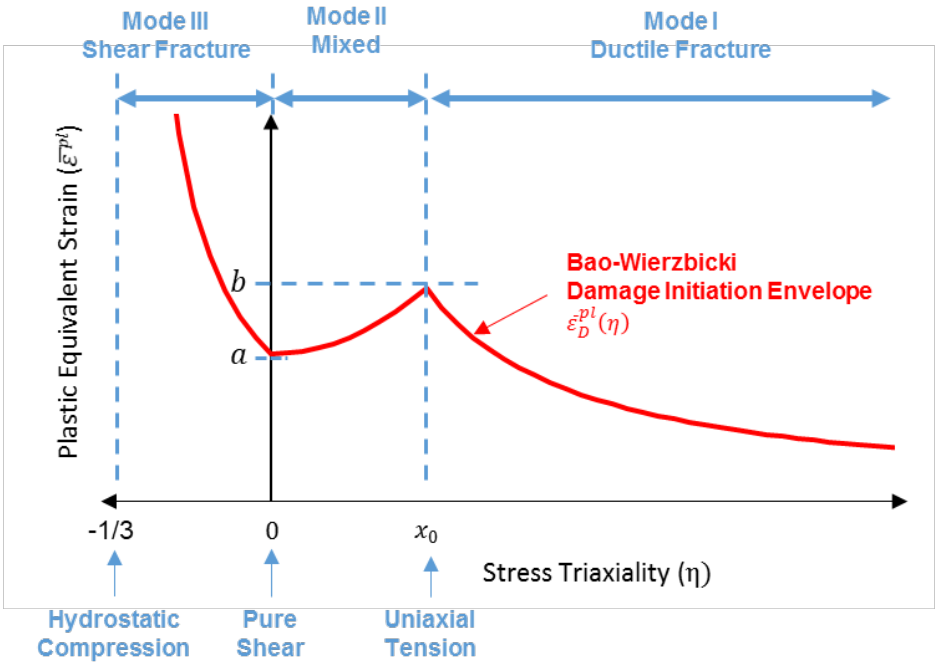

Figure 6. Schematic of B-W Fracture Locus

Three constants (i.e., a, b, x_0) govern the shape of the B-W fracture locus (Equation 2) and are calibrated based on coupon test results. The effective plastic strain to fracture in pure shear (a) corresponds to $\eta = 0$ (pure shear). The effective plastic strain to fracture in uniaxial tension (b) corresponds to the cusp of the B-W fracture locus when $\eta = x_0$.

$$\bar{\varepsilon}_D^{pl}(\eta) = \begin{cases} \dfrac{a}{1+3\cdot\eta} & -\dfrac{1}{3} \le \eta \le 0 \\ (b-a)\cdot\left(\dfrac{\eta}{x_0}\right)^2 + a & 0 \le \eta \le x_0 \\ \dfrac{b\cdot x_0}{\eta} & x_0 \le \eta \end{cases}$$

Equation 2. B-W Fracture Locus

2.2 B-W Quick Calibration

Lee & Wierzbicki (2004) and Lee (2005) developed a simplified "quick calibration" approach which requires only one uniaxial tensile geometry to estimate the entire fracture locus. The quick calibration approach is intended to be within approximately 10 percent agreement with a fracture locus that was developed using the complete set of 11 specimen geometries.

A majority of the FE analysis on tank car shell impacts summarized in Table 1 used TC128 material behaviors developed using the quick calibration method (Tests 3, 5–9).[5] In Tests 1 and 2 [1], the B-W fracture locus was calibrated from experiments conducted by Southwest Research

[5]The tank car used in Test 4 was made of A515-70 steel, not TC128.

Institute (SwRI) as part of the Next Generation Railroad Tank Car Project using a set of five specimen geometries (one pure shear and five notched tensile). Figure 7 shows a comparison of the B-W fracture loci derived from these two methods.

At high stress triaxialities, the fracture locus derived from the quick calibration method and that from tension tests using notched round bars are in reasonable agreement. However, a large discrepancy is evident between the quick calibration method and the test result for pure shear.

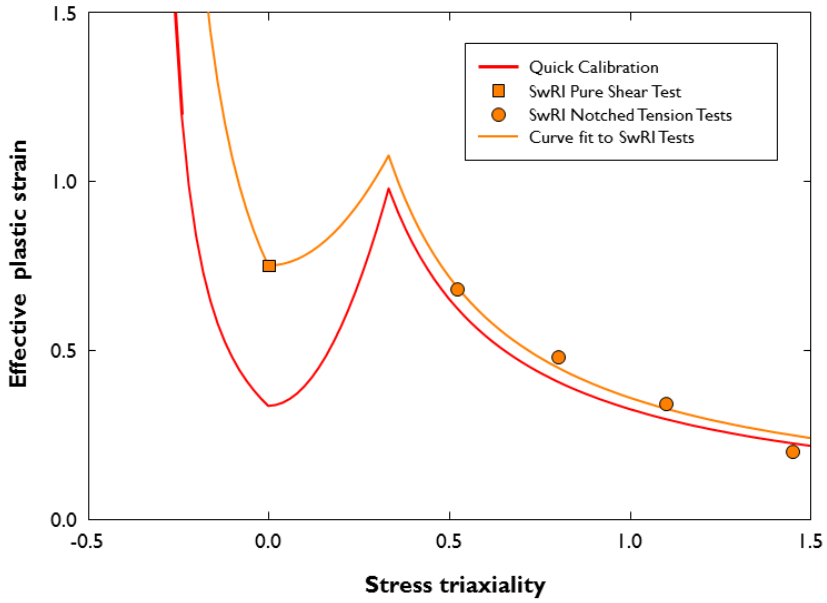

Figure 7. Comparison of B-W Fracture Loci from Quick Calibration Method and SwRI Tests

The only specimen geometry that is required to calculate the B-W fracture locus using the quick calibration method is a tensile coupon. In the US, a tensile test is typically performed in accordance with ASTM E8[6] to characterize the engineering stress-strain behaviors of a metallic specimen, including the yield strength (YS), ultimate tensile strength (UTS), elongation at break (%EB), and reduction in area (%RA). ASTM E8 includes prescribed geometries for both SRB and flat rectangular coupons (also known as dogbone,[DB]), and contains limits on the thickness of steel plates and sheets for which each coupon geometry is applicable. The quick calibration procedure using the results of SRB tensile tests allows the calculation of the B-W fracture locus constants (a, b, x_0) by measuring the initial radius (a_0), final radius (a_f), displacement at max force (δ_d), and initial gauge length (L_0) of the tensile coupon. For flat tensile coupons, the calculation of the B-W fracture locus constants is performed by measuring initial thickness (t_0) and final thickness (t_f) instead of initial and final radius. As seen in Equation 3, the quick calibration procedure also uses the hardening exponent (n) which is used to describe the plastic hardening behavior of metals by the power law. The hardening exponent is estimated as a function of engineering strain at max force.

[6] ASTM E8 / E8M-16ae1, Standard Test Methods for Tension Testing of Metallic Materials, ASTM International, West Conshohocken, PA. 2016.

SRB	DB
$n = \ln\left(1+\frac{\delta_d}{L_0}\right)$	$n = \ln\left(1+\frac{\delta_d}{L_0}\right)$
$b = 2\cdot\ln\frac{a_o}{a_f}$	$b = \frac{2}{\sqrt{3}}\cdot\ln\frac{t_o}{t_f}+\frac{2\cdot n}{\sqrt{3}}\cdot\left(\sqrt{3}-1\right)$
$x_0 = \frac{1}{3}+\frac{0.22}{b}\cdot(b-n)^{1.8}$	$x_0 = \frac{1}{\sqrt{3}}-\frac{2\cdot n}{3\cdot b}\cdot\left(\sqrt{3}-1\right)$
$a = b\cdot\left(\frac{\sqrt{3}}{2}\right)^{1/n}$	$a = b\cdot\left(\frac{\sqrt{3}}{2}\right)^{1/n}$

Equation 3. B-W Quick Calibration Procedure for Smooth Round Bar (left) and DB (right) Uniaxial Tensile Tests

Aside from the FE analysis on the tank car shell impact tests, the B-W quick calibration method has also been applied to additional applications in rail equipment crashworthiness, including failure of a cab car end frame under impact loading [22] and locomotive fuel tank integrity [23].

3. Tensile Coupon Tests and FE Analyses

During modeling of a shell impact test of a tank car, tensile coupons conforming to ASTM E8 are typically cut in the longitudinal direction. A 2-inch or 8-inch gage length is desirable so that the elongation results can be easily compared with tensile results from other material sources. Either DB or SRB geometries can be used with a 2-inch gage length while only a DB geometry can be used with an 8-inch gage length per ASTM E8. While the shell impact tests in Table 1 all had tensile coupons excised from an undamaged portion of the tank car after testing, it is preferable to have tensile test results available before conducting the test so that a calibrated material input is used in the full-scale model developed to choose the target test speed. If tensile test results are not available from the actual material then the material input needs to be estimated in a pre-test model.

If the laboratory performing the tensile testing can provide an engineering stress-strain response from the start of loading up to fracture, then a true stress-plastic equivalent strain curve can be calculated (see Section 3.1.1). If reduction in thickness/diameter measurements are also provided, then the B-W quick calibration approach discussed in Section 2.2 can be used to develop a fracture criterion. Using this methodology, a single standardized tensile test in which all the required behaviors are measured is capable of providing enough information to model the plasticity and fracture of the TC128 steel comprising the shell of a specific tested tank car.

Both ASTM E8 and the quick calibration approach to developing the B-W failure locus allow for the use of either an SRB or a DB coupon. For some of the tank cars previously-tested in FRA's program, the thickness of the shell was such that either an SRB or a DB coupon could be used that met the dimensional requirements of ASTM E8. While the failure locus and plasticity responses should be inherent material properties, as seen in Equation 3, the calculations used to develop the quick-calibration B-W failure loci differ based on whether the input data was measured using a SRB or a DB coupon. Thus, the possibility exists that the B-W failure locus developed for SRB and DB coupons excised from the same parent plate could differ. This difference, in turn, could affect the level of agreement between a simulation of a full-scale tank car impact test and the test itself, depending on which material coupon geometry was used to develop the B-W failure locus for that tank car's material.

To better understand any differences between B-W fracture loci developed using results from the different tensile geometries specified in ASTM E8, a series of different tensile coupon geometries were cut from a tested DOT-105 tank car [7] and a tested DOT-111 tank car meeting industry standard CPC-1232 [8].

Three different ASTM E8 coupon geometries were cut from each tank car: (1) DB 2-inch gage length (DB-2in), (2) DB 8-inch gage length (DB-8in), and (3) a SRB with either a 1.4-inch (SRB-1.4in) or 2-inch (SRB-2in) gage length. Because the shell in the DOT-111 tank car was not thick enough to machine to the required 0.5-inch diameter reduced section for a 2-inch gage length SRB, a 1.4-inch gage length with a 0.35-inch diameter was used instead. The DOT-105 tank car shell sample was cut into normal 2-inch gage length SRBs. Researchers tested three samples for each tank car and coupon geometry. Table 4 presents a summary of the tensile properties for the three different ASTM E8 coupon geometries from the two tested tank cars. All the coupons were tested by the same laboratory.

Table 4. Summary of ASTM E8 Tensile Test Results for Two Tank Cars

Tank Car	Geometry	YS *ksi*	UTS *ksi*	EB *%*	RA *%*	Reference
DOT-105	DB-2in	69	92	29	43	[7]
DOT-105	DB-8in	70	93	18	-	[7]
DOT-105	SRB-2in	70	94	25	49	[7]
DOT-111 (CPC-1232)	DB-2in	57	83	34	64	[8]
DOT-111 (CPC-1232)	DB-8in	59	83	23	-	[8]
DOT-111 (CPC-1232)	SRB-1.4in	60	86	32	68	[8]

Unfortunately, the test lab was not able to provide engineering stress-strain data up to fracture of the DB-8in coupons because the limit of travel for the extensometer was reached, owing to the large gage length of these coupons. Additionally, reduction in width/thickness measurements were not made before discarding the DB-8in specimens. Because of these limitations in the data, only the DB-2in and SRB specimens were used to calculate the plasticity curves and fracture loci for the TC128 samples. The complete set of tensile test results are provided in Appendix A.

The YS and UTS measurements are consistent across specimen geometries for a given tank car as expected from theory. EB cannot be compared between specimen geometries because of the localization of necking, i.e., a smaller gage length coupon undergoes necking across a larger portion of the entire gage length which results in a higher EB than larger gage length specimen. Because of this, it is useful to report EB with a standardized gage length so that comparisons between material ductility can be made.

3.1 Simulation of Tensile Tests

Commercial FE software (Abaqus/Explicit) was used to simulate the tensile tests of the various ASTM E8 coupon geometries. As the material responses developed using a coupon model were planned for implementation in the full-scale tank car models, modeling techniques for performing the coupon simulations were deliberately chosen to be similar to the modeling techniques planned for side impact puncture analyses. The same solver, element types, and mesh densities were chosen. This was done to attempt to minimize the uncertainty associated with calibrating a material response using one set of techniques, but using a different set of techniques to model puncture in the tank car impact simulation.

Within the tensile coupon FE models, the addition of a soft (1×10^{-6} lbf/in) spring represented an extensometer attached to the ends of the gage section. This spring was surrogate for an extensometer in the model and simplified the process of requesting the change-in-length of the gage section from the model.

The DOT-105 DB coupons are 0.80 inches thick and the DOT-111 DB coupons are 0.52 inches thick. Reduced integration brick elements (C3D8R) were used outside of the gage region (grey) and fully integrated brick elements (C3D8) were used inside the gage region (green). A mesh size of approximately 0.085 inches was used in the DOT-105 coupons and the DOT-111 coupons to mirror what was used in the full-scale puncture models of the tank cars. Three planes of symmetry (not shown) were applied to reduce the number of elements.

Figure 8 shows FE models of the DB-2in coupons from the DOT-105 (top) and DOT-111 (bottom) tank cars.

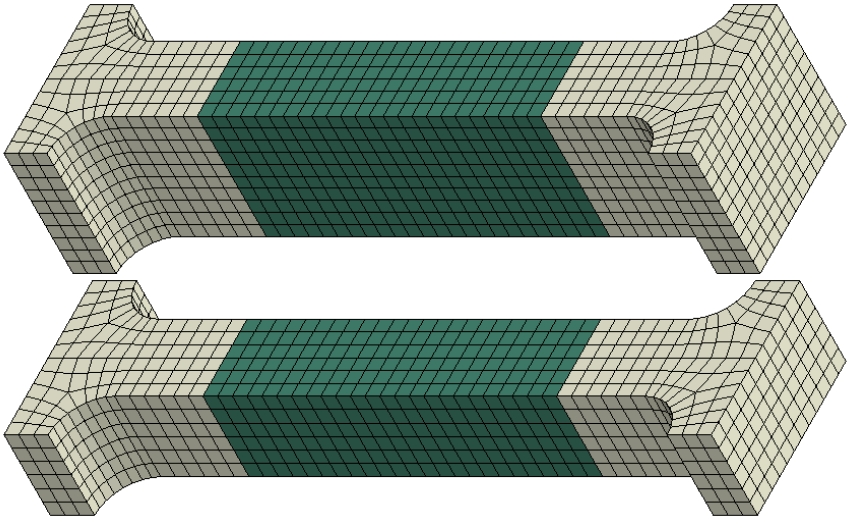

Figure 8. FE Model of Flat Tensile (DB) Coupons

Figure 9 shows FE models of the DB-8in from the DOT-105 (top) and DOT-111 (bottom) tank cars.

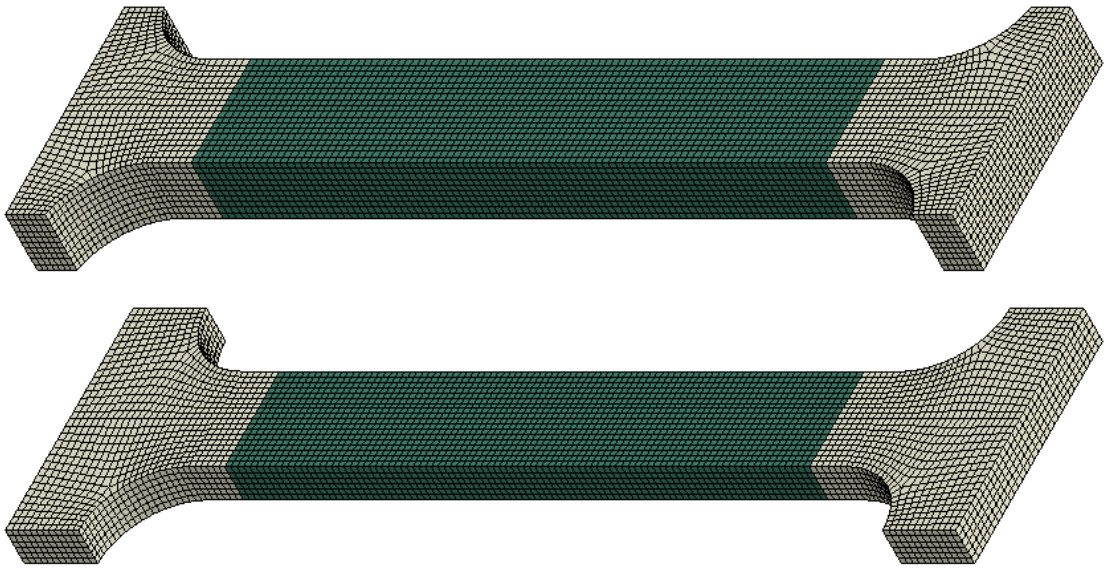

Figure 9. FE Model of Flat Tensile (DB) Coupons

Figure 10 shows FE models of the SRB-2in from the DOT-105 (top) and SRB-1.4in from the DOT-111 (bottom). The mesh size was lowered to 0.05 inches for the SRB-1.4in model because of the reduced diameter (0.35 inches). A minimum of three elements across the radius was needed to capture necking.

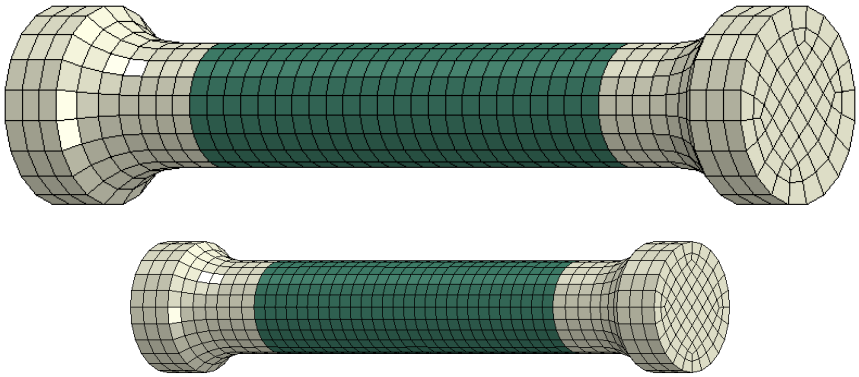

Figure 10. FE Model of SRB Coupons

From a mesh uniformity perspective, DB specimens are desirable because they result in a regularized brick element mesh. SRB specimens are unable to maintain a constant brick element size across the fracture surface. However, as discussed later in Section 3.1.2, the SRB version of the B-W quick calibration procedure results in a B-W fracture locus that does not need to be modified for the tensile coupon FE model to have the correct elongation at break.

Table 5 summarizes the meshes and geometries for each ASTM E8 tensile coupon model. The number of brick elements of each type (C3D8 and C3D8R) is reported from the 1/8 symmetric model while the thickness, width, and diameters are reported for the full-sized geometry.

Table 5. Summary of ASTM E8 Coupon FE Models

Geometry	**Tank Car**	**# of Elements**	**Mesh Size** *inches*	**Thickness or Diameter** *inches*	**Width** *inches*
DB-2in	DOT-105	C3D8: 180 C3D8R: 230	0.085	0.80	0.5
DB-2in	DOT-111	C3D8: 108 C3D8R: 138	0.085	0.52	0.5
DB-8in	DOT-105	C3D8: 2,115 C3D8R: 1,355	0.085	0.80	1.5
DB-8in	DOT-111	C3D8: 1,269 C3D8R: 1,179	0.085	0.52	1.5
SRB-2in	DOT-105	C3D8: 132 C3D8R: 97	0.085	0.50	-
SRB-1.4in	DOT-111	C3D8: 210 C3D8R: 129	0.050	0.35	-

For each coupon geometry, the tensile test was simulated by placing a displacement boundary condition at the top of the widest portion of the coupon. This simulated the action of the top grip during an actual tensile test. The displacement was gradually increased, with the applied force needed to attain that displacement being calculated by the simulation.

3.1.1 Plasticity

Abaqus/Explicit requires metal plasticity to be defined in terms of true stress (σ_t) and $\bar{\varepsilon}^{pl}$. The plastic behavior of each material model of TC128 was input to the Abaqus model as isotropic hardening using a discrete number of data points. True stress can be calculated from the nominal stress-strain tensile coupon data according to Equation 4.

$$\sigma_{true} = \sigma_{nom} \cdot (1 + \varepsilon_{nom})$$

$$\bar{\varepsilon}^{pl} = \ln(1 + \varepsilon_{nom}) - \frac{\sigma_t}{E}$$

σ_{nom} nominal (engineering) stress

ε_{nom} nominal (engineering) strain

σ_t true stress

$\bar{\varepsilon}^{pl}$ plastic equivalent strain

Equation 4. True Stress-strain Transformation

Figure 11 shows the results of using Equation 4 to calculate σ_t and $\bar{\varepsilon}^{pl}$ from representative DB and SRB coupons cut from each tank car. The calculations could not be performed on the DB-8in because the extensometer used in the tests reached its travel limit before fracture occurred.

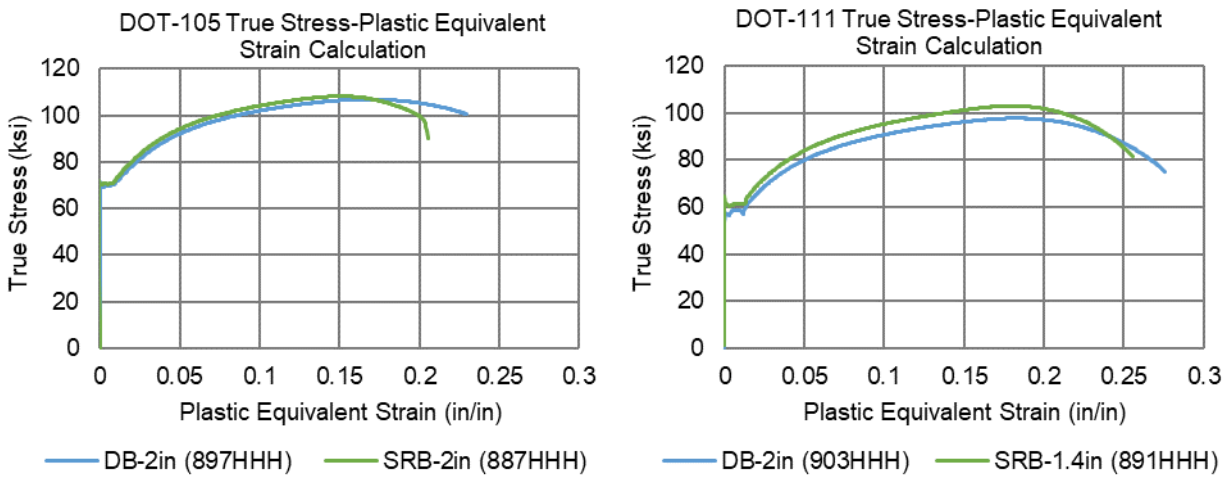

Figure 11. True Stress-Plastic Equivalent Strain Calculations from DOT-105 (left) and DOT-111 (right) ASTM E8 Coupons

The calculation of σ_t versus $\bar{\varepsilon}^{pl}$ is only valid up to the point where necking occurs; afterward, necking dominates the observed response resulting in a reduction in hardening that is non-physical. Because the FE model requires a plastic hardening relationship that is valid for $\bar{\varepsilon}^{pl}$ strains beyond the point where necking occurs, the σ_t versus $\bar{\varepsilon}^{pl}$ relationship was extrapolated for $\bar{\varepsilon}^{pl}$ beyond the corresponding nominal strain at max force using the Swift model [24] also referred to as the power law.

$$\sigma_t^{Swift}(\bar{\varepsilon}^{pl}) = A \cdot (\varepsilon_0 + \bar{\varepsilon}^{pl})^n$$

Equation 5. Swift (power law) Model of Plastic Hardening

Figure 12 shows the σ_t versus $\bar{\varepsilon}^{pl}$ inputs used to define plastic hardening in the tensile coupon models. The inputs were created by manually selecting points on the calculated curves in Figure 11 up to the strain at max force. Afterwards the Swift model was used to extrapolate the curve for high strains.

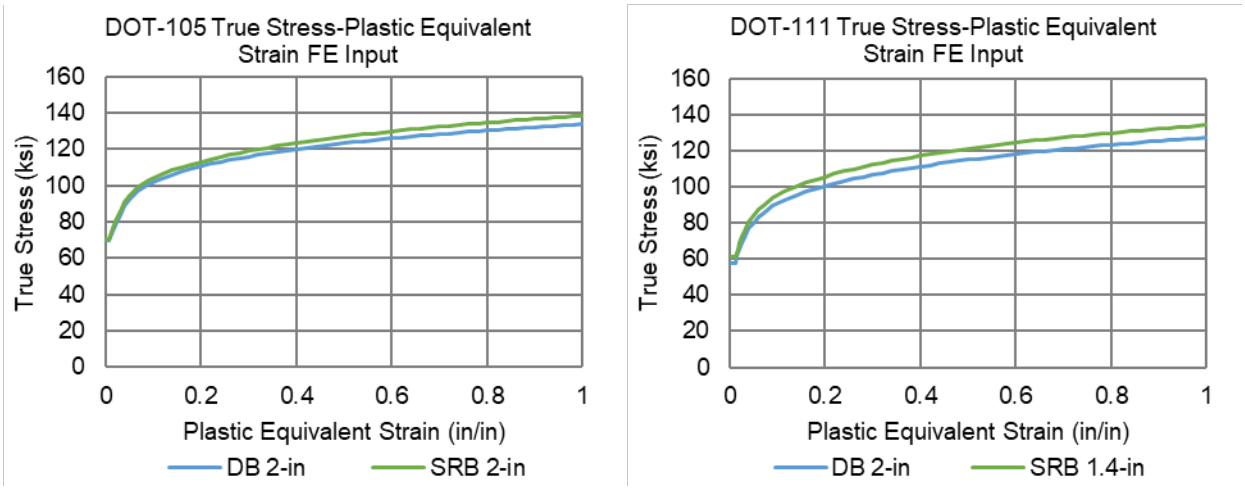

Figure 12. True Stress-Plastic Equivalent Strain FE Input of DOT-105 (left) and DOT-111 (right) ASTM E8 Coupons

Constants for the Swift model were determined by linear regression in the region of the calculated σ_t versus $\bar{\varepsilon}^{pl}$ curve between the Lüders band (the portion of near-constant stress for increasing strain at the onset of plasticity) and the value of $\bar{\varepsilon}^{pl}$ corresponding to the nominal strain at max force. Table 6 gives the constants used for the Swift model extrapolation of the plasticity curve inputs for the tensile coupon models. In all cases plastic equivalent strain offset constant, ε_0, was constrained to zero to simplify the regression.

Table 6. Swift (power law) Model Constants for Plasticity Curve Inputs in FE Models

	DOT-105		**DOT-111**	
	A	*n*	*A*	*n*
DB-2in	133.84	0.11883	127.27	0.14753
SRB	138.38	0.12484	134.15	0.14876

The plastic stress-strain response of a material should be an inherent property of the material, and therefore independent of the coupon geometry used to measure the response. For each tank car, the values of *A* and *n*, are close to one another, but are not identical. In general, the shapes of the resulting σ_t versus $\bar{\varepsilon}^{pl}$ responses are close to one another. For both cars, the DB-2in coupon resulted in slightly smaller values of *A* and *n* than the SRB coupons.

3.1.2 Fracture

Abaqus/Explicit implements the B-W fracture locus using the **Ductile Damage* keyword. This keyword requires ductile damage to be defined in terms of $\bar{\varepsilon}^{pl}$ and η. The B-W criterion (Equation 2) is used to specify a damage initiation curve and the constants are calibrated using the B-W quick calibration procedure (Equation 3) for either DB or SRB coupons. The B-W locus for a given TC128 material is discretized by calculating the $\bar{\varepsilon}^{pl}$ for a given η by using the calibrated constants. The $\bar{\varepsilon}^{pl}$ versus η curve can then be input to Abaqus/Explicit in tabular form.

Table 7 summarizes the average measurements from tensile tests needed to perform the B-W quick calibration procedure. For DB coupons, the measurements include initial thickness (t_0), final thickness (t_f), and displacement at max force (δ_d). For SRB coupons, initial and final thicknesses are replaced with initial radius (a_0) and final radius (a_f).

Table 7. ASTM E8 Average Tensile Test Results Used for B-W Quick Calibration

	DOT-105			DOT-111		
	δ_d *inches*	t_0 or a_0 *inches*	t_f or a_f *inches*	δ_d *inches*	t_0 or a_0 *inches*	t_f or a_f *inches*
DB-2in	0.30363	0.80493	0.614	0.30417	0.52327	0.303
SRB	0.25469	0.25143	0.18005	0.22059	0.1763	0.1001

Figure 13 shows the B-W fracture loci created using the quick calibration procedure with the DB-2in and SRB coupon geometries and the values shown in Table 7. The quick calibration procedure requires the strain or displacement at max stress or force and the reduction in thickness or diameter. Using the SRB tensile test results and corresponding SRB quick calibration equations, a B-W locus (green line) was created that could be applied to the SRB model which resulted in a correct elongation at break (within 5%) for both the DOT-105 and DOT-111 coupons. However, when the corresponding approach was taken to create a B-W locus (blue line) with the DB 2-inch gage length test results and equations, the resulting elongation at break in the DB 2-inch gage length model was approximately 15 percent lower than measured.

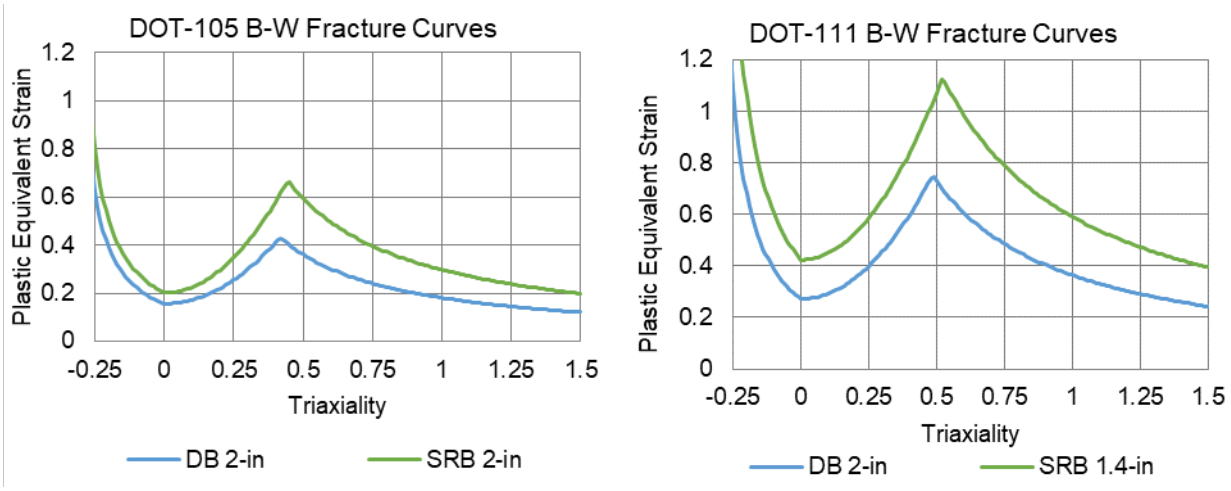

Figure 13. B-W Fracture Loci from Quick Calibration of DOT-105 (left) and DOT-111 (right) ASTM E8 Tensile Coupons

Table 8 gives the B-W criterion constants for the curves shown in Figure 13. The DB-2in B-W loci were modified by applying a linear scaling factor (β) to the measured reduction in thickness (t_f) in Table 7. The reduction in thickness measurement was chosen for modification because the DOT-105 and DOT-111 DB coupons were much thicker than the original DB coupons used by Lee (2005) to develop the B-W quick calibration procedure. Lee used a plane stress assumption when developing the DB quick calibration equations (Equation 3) which is not valid for coupons that have a larger thickness than width [11]. The linear scaling factors were determined iteratively by rerunning the coupon model until the elongation at break in the model was within ±5% agreement with the average test results.

Table 8. B-W Fracture Locus Constants DOT-105 (left) and DOT-111 (right) TC128 Steels

	DOT-105				DOT-111			
	a	b	x_0	β	a	b	x_0	β
DB-2in	0.15618	0.43212	0.41772	1	0.27173	0.75055	0.48529	1
DB-2in (Modified)	0.24931	0.68939	0.47735	0.8	0.40906	1.1299	0.51620	0.72
SRB	0.20116	0.66789	0.44491	1	0.42356	1.1320	0.52271	1

Figure 14 shows the modified DB B-W loci (orange line) with the unmodified DB (blue line) and SRB (green line) curves for comparison. It is noteworthy that the modified DB curves ended up being in close agreement with the SRB curves.

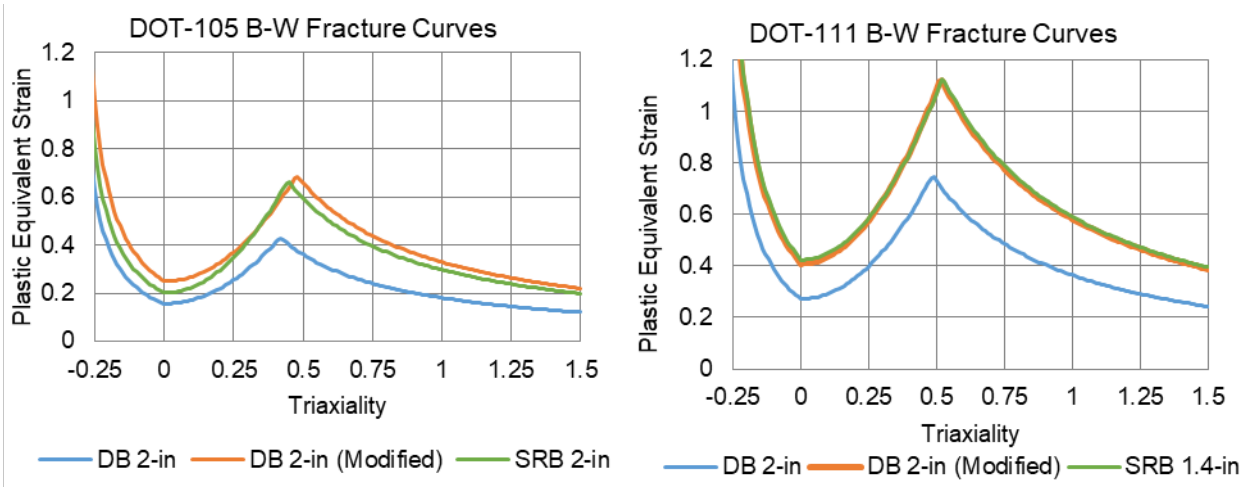

Figure 14. Modified DB-2in B-W Fracture Loci from Quick Calibration of DOT-105 (left) and DOT-111 (right) ASTM E8 Tensile Coupons

For ductile metals in Abaqus, the damage threshold of an integration point is reached when the ductile criterion (ω_D) reaches a value of 1. According to Equation 6, ω_D is calculated by integrating the change in $\bar{\varepsilon}^{pl}$ by effective strain to fracture as a function of triaxiality, i.e., the B-W fracture locus from Equation 2.

$$\omega_D = \int \frac{d\bar{\varepsilon}^{pl}}{\bar{\varepsilon}_D^{pl}(\eta)}$$

Equation 6. Calculation of Ductile Criterion (ω_D) in Abaqus

After ω_D reaches a value of 1 the stiffness of the element is degraded and eventually removed according to the damage progression in the material definition. In this report, an energy-based damage progression was calibrated by iteratively rerunning the model to give qualitative agreement with the drop in nominal stress as the tensile specimens fractured. A value of 850 in-lbf/in^2 was chosen for the DOT-105 and DOT-111 DB-2in FE models and the DOT-105 SRB-2in models which all used a mesh size of 0.085 inches. The progression was reduced to 300 in-lbf/in^2 for the DOT-111 SRB-1.4 in model which had a mesh size of 0.05 inches.

3.2 Comparison of FE Analyses and Test Results

Figure 15 shows the nominal stress-strain responses from the DB-2in tensile tests and the corresponding FE analyses of the DOT-105 and DOT-111 DB-2in models. The DB-2in material models were calibrated in terms of plasticity (Section 3.1.1) and fracture (Section 3.1.2) using the DB-2in test results. The FE results are in near perfect agreement with the test results up to damage initiation, but the B-W quick calibration procedure results in early damage initiation with thick DB geometries. It should be noted that only one DOT-105 DB-2in test curve is shown because the extensometer data from the other samples did not agree with manual measurement of the elongation at break on the fractured specimens.

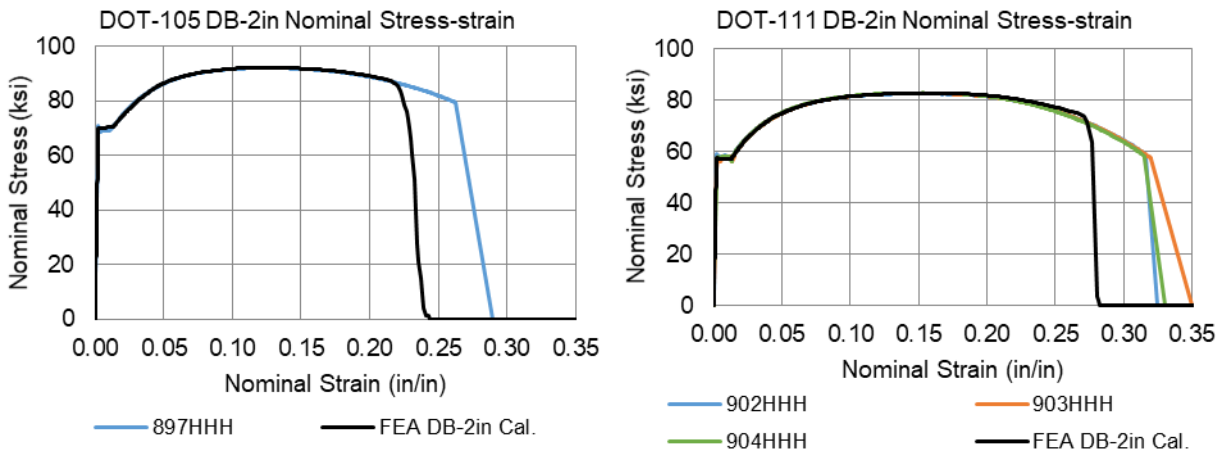

Figure 15. Nominal Stress-Strain Test and FE Results from DOT-105 (left) and DOT-111 (right) DB-2in Specimens

Figure 16 shows the nominal stress-strain responses from the DB-2in tensile tests and the corresponding FE analyses of the DOT-105 and DOT-111 DB-2in models with modified B-W fracture loci. As described in Section 3.1.2, the fracture loci were iteratively modified until the correct elongation at break was achieved in the models.

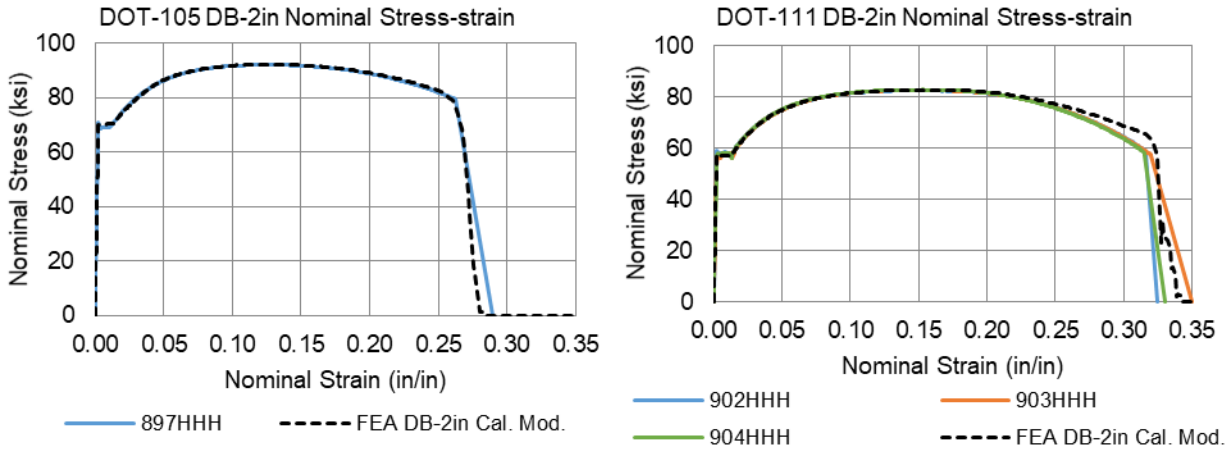

Figure 16. Nominal Stress-Strain Test Results from DOT-105 (left) and DOT-111 (right) DB-2in Specimens and FE Results with Modified DB-2in Material Input

Figure 17 shows the DB-2in test results alongside results from the DB-2in FE models that were run using material models calibrated with the SRB test results. The elongation at break is in near perfect agreement while using an unmodified B-W fracture locus calibrated with a different tensile geometry. The UTS and YS are slightly overestimated in the FE model which could be due to errors in measuring cross-sectional area prior to tensile testing.

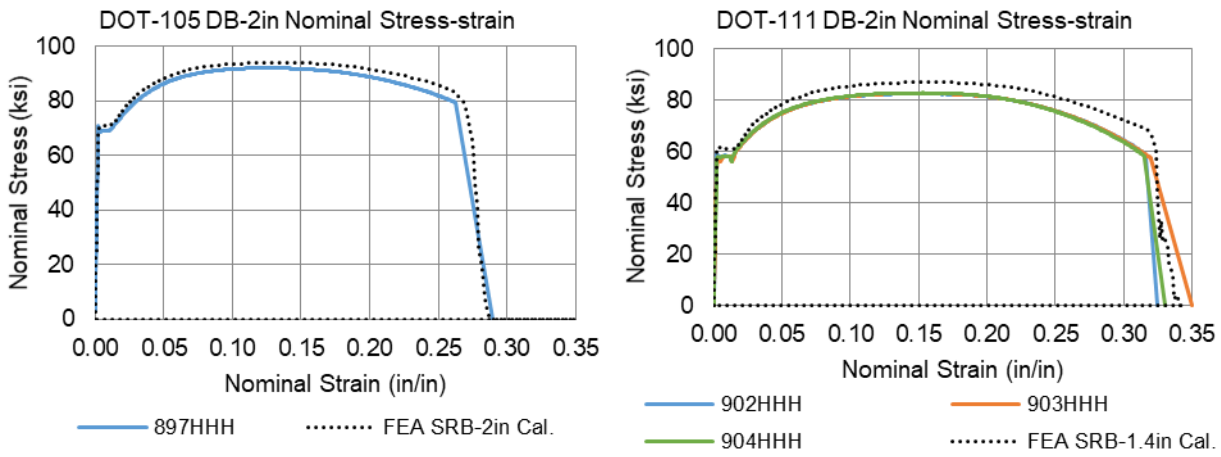

Figure 17. Nominal Stress-Strain Test Results from DOT-105 (left) and DOT-111 (right) DB-2in Specimens and FE Results with SRB Material Input

Figure 18 shows the nominal stress-strain responses from the SRB tensile tests and the corresponding FE analyses of the DOT-105 and DOT-111 SRB models. The SRB material models were calibrated in terms of plasticity (Section 3.1.1) and fracture (Section 3.1.2) using the SRB test results. A straight line is drawn from the last nominal stress-strain data point available from the test machine to the measured elongation at break.

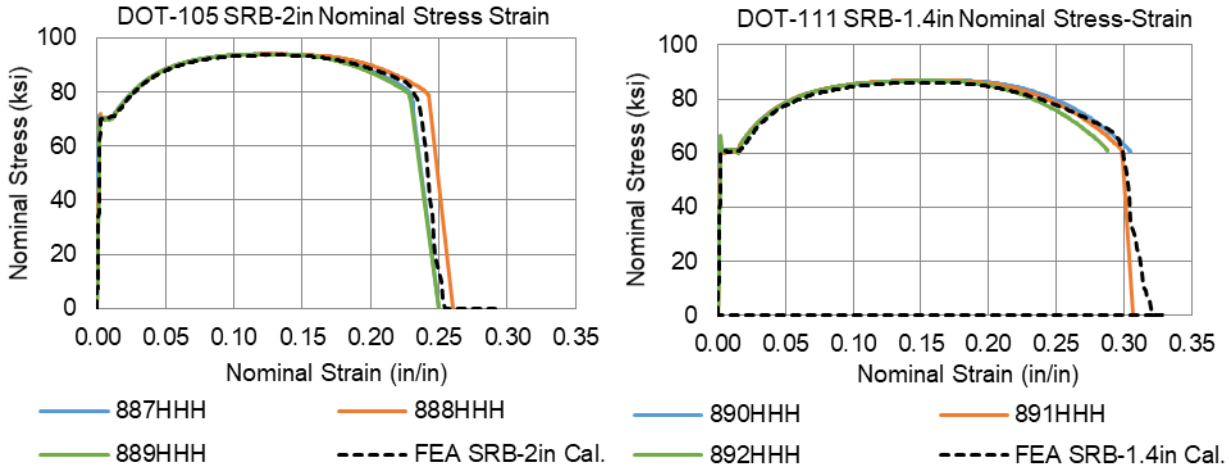

Figure 18. Nominal Stress-Strain Test and FE Results from DOT-105 (left) and DOT-111 (right) SRB Specimens

Figure 19 shows the SRB test results presented, above but also shows results from the FE model of the SRB geometry when run with the material input calibrated from the DB-2in test results with modified fracture loci. The material models calibrated with DB geometries are still in good agreement with the SRB test results; however, YS and UTS are slightly underestimated as discussed above.

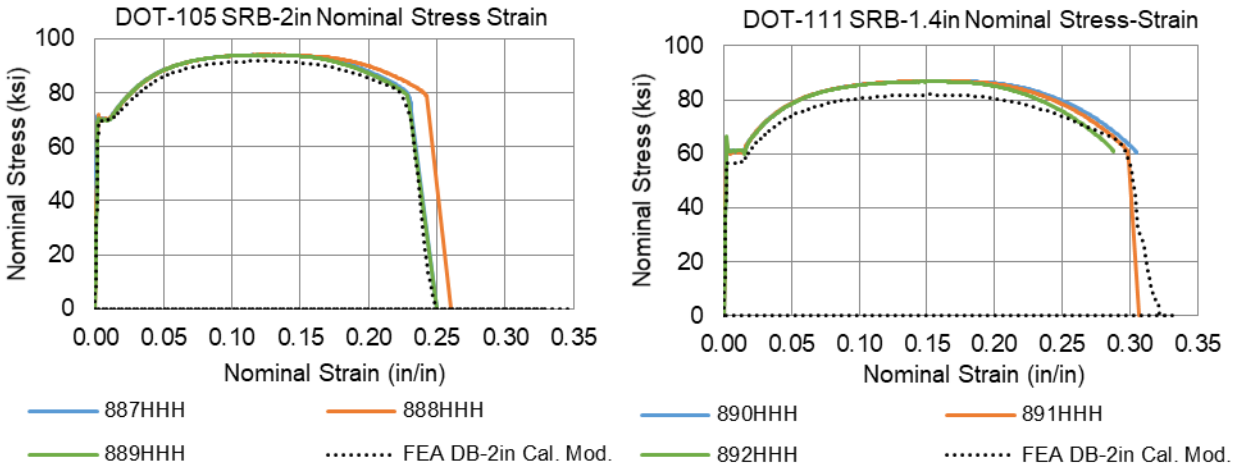

Figure 19. Nominal Stress-Strain Test Results from DOT-105 (left) and DOT-111 (right) SRB Specimens and FE Results with Modified DB-2in Material Input

Figure 20 shows the nominal stress-strain responses from the DB-8in FE analyses of the DOT-105 and DOT-111 DB-8in models. A DB-8in material model was not calibrated because a complete set of the necessary tensile results were unavailable. For the sake of comparison, the FE material models that were calibrated using the DB-2in and SRB test results are shown for comparison for each tank car. Because an 8-inch extensometer was unavailable for testing, the average tensile results for UTS and EB are shown. The agreement between FE results and the average test results indicates that the material models calibrated using other uniaxial tensile coupon geometries are valid.

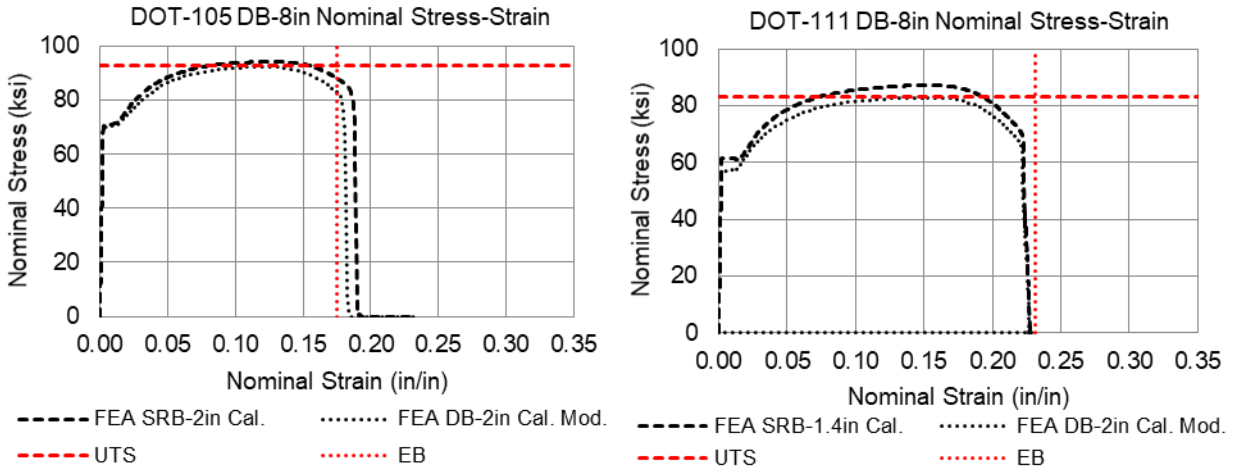

Figure 20. Nominal Stress-Strain Test and FE Results from DOT-105 (left) and DOT-111 (right) DB-8in Specimens

4. Conclusion

This report documents the efforts of Volpe to characterize the fracture of AAR TC128, Grade B steel for full scale puncture modeling of side impact tests from April 5, 2019, to August 20, 2020. This testing and analysis supports FRA's tank car research program to provide the technical basis for rulemaking on enhanced and alternative performance standards for tank cars.

The B-W quick calibration procedure was used to create B-W fracture loci with standardized ASTM E8 tensile coupon geometries. The coupon geometries consisted of flat (DB) and round (SRB) uniaxial tensile coupons cut in the longitudinal direction from undamaged portions of the tank cars. The DB coupons either had 2-inch or 8-inch gage lengths for each tank car. The SRB coupons had a 2-inch gage length for the DOT-105 and a 1.4-inch gage length for the DOT-111 tank car.

B-W fracture loci were created for the DB-2in and SRB coupon geometries for each tank car but a fracture locus could not be created for the DB-8in coupons because key tensile properties were unavailable. Plastic hardening inputs for the FE models were also created to be used in conjunction with the fracture loci for the DB-2in and SRB coupons.

The SRB tensile properties resulted in B-W fracture loci that, when applied to the SRB FE model, resulted in a correct elongation at break (within 5%) for both the DOT-105 and DOT-111 coupons. However, the DB-2in tensile properties resulted in a B-W fracture loci that was 15 percent lower than measured when applied to the DB-2in FE model. The DB-2in B-W fracture loci were subsequently modified in an iterative fashion to reach agreement (±5%) with the elongation at break from the test results. The DB-2in B-W fracture loci were modified by linearly scaling the final thickness results.

While DB specimens are desirable because they result in uniform brick element meshes and require less machining, the plane stress assumption used in the DB version of the B-W quick calibration procedure cannot be upheld due to the thickness of the specimens. Even though SRB specimens are unable to maintain a constant brick element size across the fracture surface and require more machining, the SRB version of the B-W quick calibration procedure resulted in a B-W fracture locus that does not need to be modified to result in tensile coupon FE results with the correct elongation at break.

Therefore, it is recommended to use SRB coupons when following the B-W quick calibration procedure to create a fracture locus. A DB coupon geometry can be used in addition to report a 2-inch gage length elongation at break if it is not feasible to machine a 0.5-inch diameter SRB specimen. The DB tensile results can also act as a FE model validation case for the B-W fracture locus calibrated using the SRB tensile results. With additional tensile test results from a variety of TC128 thicknesses, future work can examine whether a relationship for the scaling factor beta used with DB coupons can be established.

5. References

[1] Kirkpatrick, S., "Detailed Puncture Analyses of Various Tank Car Designs: Final Report - Revision 1," Applied Research Associates, Inc., Mountain View, CA, January 2010.

[2] Carolan, M., Jeong, D., Perlman, B., Murty, Y., Namboordri, S., Kurtz, R., Elzey, R., Ananikitpaiboon, S., Tunna, L., & Fries, R., "Application of Welded Steel Sandwich Panels for Tank Car Shell Impact Protection," U.S. Department of Transportation, Federal Railroad Administration, Technical Report No. DOT/FRA/ORD-13/19, Washington, DC, 2013.

[3] Kirkpatrick, S., Rakoczy, P., MacNeill, R., & Anderson, A., "Side Impact Test and Analyses of a DOT-111 Tank Car," U.S. Department of Transportation, Technical Report No. DOT/FRA/ORD-15/30, Washington, DC, 2015.

[4] Rakoczy, P., & Carolan, M., "Side Impact Test and Analysis of a DOT-112 Tank Car," U.S. Department of Transportation, Federal Railroad Administration, Technical Report No. DOT/FRA/ORD-16/38, Washington, DC, 2016.

[5] Carolan, M., & Rakoczy, P., "Side Impact Test and Analysis of a DOT-105 Tank Car," U.S. Department of Transportation, Federal Railroad Administration, Technical Report No. DOT/FRA/ORD-19/12, Washington, DC, 2019.

[6] Rakoczy, P., Carolan, M., Gorhum, T., & Eshraghi, S., "Side Impact Test and Analyses of a DOT-117 Tank Car," U.S Department of Transportation, Federal Railroad Administration, Technical Report No. DOT/FRA/ORD-19/13, Washington, DC, 2019.

[7] Wilson, N., Eshraghi, S., Trevithick, S., Carolan, M., & Rakoczy, P., "Side Impact Test and Analyses of a DOT-105 Tank Car – 6 X 6 Inch Indenter," U.S. Department of Transportation, Federal Railroad Administration, Technical Report No. DOT/FRA/ORD-20/38, Washington, DC, 2020.

[8] Eshraghi, S., Trevithick, S., Carolan, M., Rakoczy, P., & Wilson, N., "Side Impact Test and Analyses of a DOT-111 (CPC-1232) Tank Car," U.S. Department of Transportation, Federal Railroad Administration, Technical Report No. DOT/FRA/ORD-20/43, Washington, DC, 2020.

[9] Bao, Y., & Wierzbicki, T., "On fracture locus in the equivalent strain and stress triaxiality space," *International Journal of Mechanical Sciences,* vol. 46, pp. 81-98, 2004.

[10] Lee, Y., & Wierzbicki, T., "Quick Fracture Calibration for Industrial Use," Impact Crashworthiness Laboratory, Massachusetts Institute of Technology, Technical Report No. 115, 2004.

[11] Lee, Y.-W., "Fracture Prediction in Metal Sheets," Thesis Submitted to Massachusetts Institute of Technology, 2005.

[12] Hancock, J., & Mackenzie, A., "On the mechanics of ductile fracture in high-strength steels subjected to multi-axial stress states," *Journal of the Mechanics and Physics of Solids 24,* vol. 24, no. 2-3, pp. 147-160, 1976.

[13] Le Roy, G., Embur, J., Edwards, ., & Ashby, M., "A model of ductile fracture based on the nucleation and growth of voids," *Acta Materialia,* vol. 29, no. 8, pp. 1509-1522, 1981.

[14] Johnson, G., & Cook, W., "Fracture characteristics of three metals subject to various strains, strain rates, temperatures and pressures," *Engineering Fracture Mechanics,* vol. 21, no. 1, pp. 31-48, 1985.

[15] Gurson, A. L., "Continuum Theory of Ductile Rupture by Void Nucleation and Growth: Part I - Yield Criteria and Flow Rules for Porous Ductile Media," *Journal of Engineering Materials and Technology ,* vol. 99, pp. 2-15, 1977.

[16] Tvergaard, V., "Influence of voids on shear band instabilities under plane strain conditions," *International Journal of Fracture Mechanics,* vol. 17, pp. 389-407, 1981.

[17] Barsoum, I., & Faleskog, J., "Rupture mechanics in combined tension and shear—Experiments," *International Journal of Solids and Structures,* vol. 44, no. 6, pp. 1768-1786, 2007.

[18] Bai, Y., & Wierzbicki, T., "A new model of metal plasticity and fracture with pressure and Lode dependence," *International Journal of Plasticity,* vol. 24, no. 6, pp. 1071-1096, 2008.

[19] Mohr, D., & Ebnoether, F., "Plasticity and fracture of martensitic boron steel under plane stress conditions," *International Journal of Solids and Structures ,* vol. 46, no. 20, pp. 3535-3547, 2009.

[20] Dunand, M., & Mohr, D., "Hybrid experimental–numerical analysis of basic ductile fracture experiments for sheet materials," *International Journal of Solids and Structures,* vol. 47, no. 9, pp. 1130-1143, 2010.

[21] Faleskog, J., & Barsoum, I., "Tension–torsion fracture experiments—Part I: Experiments and a procedure to evaluate plastic strain," *International Journal of Solids and Structures,* vol. 50, no. 25-26, pp. 4241-4257, 2013.

[22] Stringfellow, R., & Paetsch, C., "Modeling Material Failure During Cab Car End Frame Impact," in *2009 Joint Rail Conference, JRC2009-63054*, 2009.

[23] Jacobsen, K., Llana, P., Carolan, M., & Sullivan, L., "Fuel Tank Integrity Research: Fuel Tank Analyses and Test Plans," in *Proceedings of the 2013 ASME/IEEE/ASCE Joint Rain Conference*, JRC2013-2425, Knoxville, TN, 2013.

[24] Swift, H., "Plastic instability under plane stress," *Journal of Mechanics and Physics of Solids,* vol. 1, no. 1, pp. 1-18, 1952.

[25] Yu, H., Jeong, D., Gordon, J., & Tang, Y., "Analysis of Impact Energy to Fracture Unnotched Charpy Specimens Made from Railroad Tank Car Steel," in *Proceedings of the*

2007 ASME Rail Transportation Division Fall Technical Conference, RTDF2007-46038, Chicago, IL, 2007.

[26] Tang, Y., Yu, H., Gordon, J., & Jeong, D., "Analysis of Railroad Tank Car Shell Impacts Using Finite Element Method," in *IEEE/ASME/ASCE 2008 Joint Rail Conference*, JRC2008-63014, Wilmington, DE, 2008.

[27] Nahson, K., & Hutchinson, J., "Modification of the Gurson Model for shear failure," *European Journal of Mechanics A/Solids,* vol. 27, pp. 1-17, 2008.

[28] Wierzbicki, T., & Xue, L., "On the Effect of the Third Invariant of the Stress Deviator on Ductile Fracture," Impact and Crashworthiness Laboratory, Massachusetts Institute of Technology, Technical Report No. 136, Cambridge, MA, 2005.

[29] Kirkpatrick, S., & McKeighan, P., "Correlating Material Properties to Puncture Resistance to Enhance the Safety and Security of Tank Cars," March 2018.

[30] Paredes, M., Grolleau, V., & Wierzbicki, T., "On ductile fracture of 316L stainless steels at room cryogenic temperature level: An engineering approach to determine material parameters," *Materialia,* vol. 10, p. 100624, 2020.

[31] Voce, E., "The relationship between stress and strain for homogeneous deformations," *Journal of the Institute of Metals,* vol. 74, pp. 537-562, 1948.

[32] Bai, Y., & Wierzbicki, T., "Application of extended Mohr-Coulomb criterion to ductile fracture," *International Journal of Fracture,* vol. 161, no. 1, pp. 1-20, 2010.

Appendix A.
ASTM E8 Tensile Test Results

Table A1. ASTM E8 Tensile Results of Flat Coupons with 2-inch Gage Length (DB-2in)

Property	**Units**	**DOT-105 DB-2in**			**DOT-111 DB-2in**		
Test Log #	-	896HHH	897HHH	898HHH	902HHH	903HHH	904HHH
UTS	*ksi*	92.0	92.1	92.4	82.6	82.8	82.9
0.2% YS	*ksi*	69.4	69.1	69.5	57.0	56.8	57.4
Elong.	*%*	29	29	30	33	35	33
RA	*%*	42	43	44	64	66	63
Modulus	*msi*	30.3	29.8	29.7	31.2	27.5	28.4
Ult. Load	*lbf*	36684	37293	37410	21758	21797	21816
0.2% YLD.	*lbf*	27671	27954	28148	14999	14955	15094
Orig. Width	*in*	0.4962	0.5020	0.5032	0.5027	0.5033	0.5032
Final Width	*in*	0.3786	0.3752	0.3703	0.3130	0.3030	0.3155
Orig. Thick	*in*	0.8036	0.8064	0.8048	0.5238	0.5233	0.5227
Final Thick	*in*	0.6132	0.6165	0.6123	0.3070	0.2940	0.3080
4D Orig. GL	*in*	2.00	2.00	2.00	2.00	2.00	2.00
4D Final GL	*in*	2.58	2.58	2.59	2.65	2.70	2.66

Table A2. ASTM E8 Tensile Results of Flat Coupons with 8-inch Gage Length (DB-8in)

Property	**Units**	**DOT-105 DB-8in**			**DOT-111 DB-8in**		
Test Log #	-	893HHH	894HHH	895HHH	899HHH	900HHH	901HHH
UTS	*ksi*	92.8	91.7	93.1	82.7	83.3	83.4
0.2% YS	*ksi*	70.0	69.3	70.9	59.5	58.7	58.8
Elong	*%*	18	17	18	24	23	23
Modulus	*msi*	30.9	29.6	31.0	14.5	30.1	29.7
Ult. Load	*lbf*	111644	111399	111735	65200	65674	65665
0.2% YLD.	*lbf*	84271	84175	85082	46901	46237	46331
Orig. Width	*in*	1.5036	1.5050	1.5046	1.5054	1.5052	1.5046
Final Width	*in*	-	-	-	-	-	-
Orig. Thick	*in*	0.8002	0.8076	0.7978	0.5238	0.5236	0.5234
Final Thick	*in*	-	-	-	-	-	-
4D Orig. GL	*in*	8.00	8.00	8.00	8.00	8.00	8.00
4D Final GL	*in*	9.41	9.38	9.40	9.91	9.81	9.83

Table A3. ASTM E8 Tensile Results of Round Coupons with 2-inch (SRB-2in) and 1.4-inch (SRB-1.4in) Gage Lengths

Property	**Units**	**DOT-105 SRB-2in**			**DOT-111 SRB-1.4in**		
Test Log #	-	887HHH	888HHH	889HHH	890HHH	891HHH	892HHH
UTS	*ksi*	94.1	94.1	94.0	87.0	86.9	86.7
0.2% YS	*ksi*	70.2	70.6	70.1	61.1	61.4	60.9
Elong	*%*	25	26	25	31	31	29
RA	*%*	49	48	49	68	68	67
Modulus	*msi*	51.9	39.0	36.5	33.4	40.5	34.6
Ult. Load	*lbf*	18676	18705	18680	8499	8495	8461
0.2% YLD.	*lbf*	13936	14031	13931	5974	5995	5944
Orig. Dia.	*in*	0.5027	0.5030	0.5029	0.3527	0.3527	0.3524
Final Dia.	*in*	0.3574	0.3624	0.3605	0.1992	0.2004	0.2010
4D Orig. GL	*in*	2.00	2.00	2.00	1.40	1.40	1.40
4D Final GL	*in*	2.49	2.52	2.49	1.84	1.83	1.81

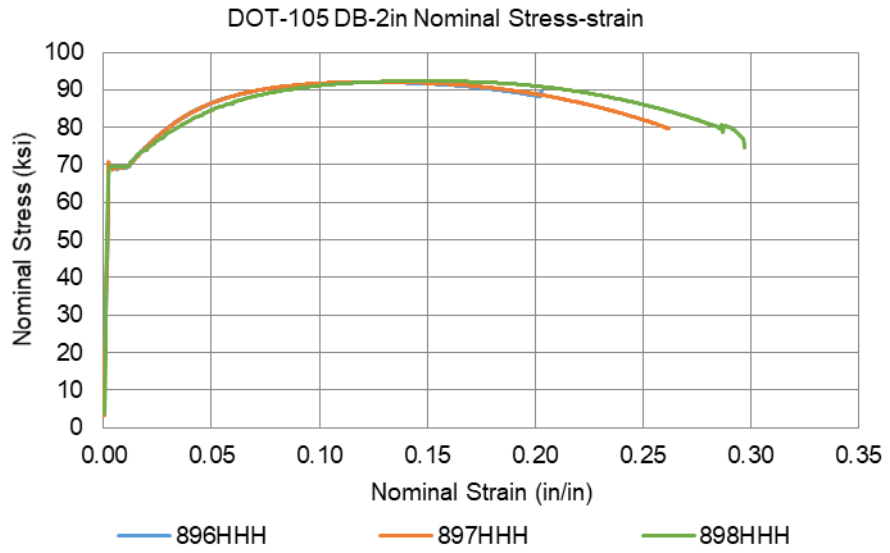

Figure A1. Nominal Stress-Strain Tensile Results from Flat 2-inch Gage Length Coupons (DB-2in) Cut from DOT-105

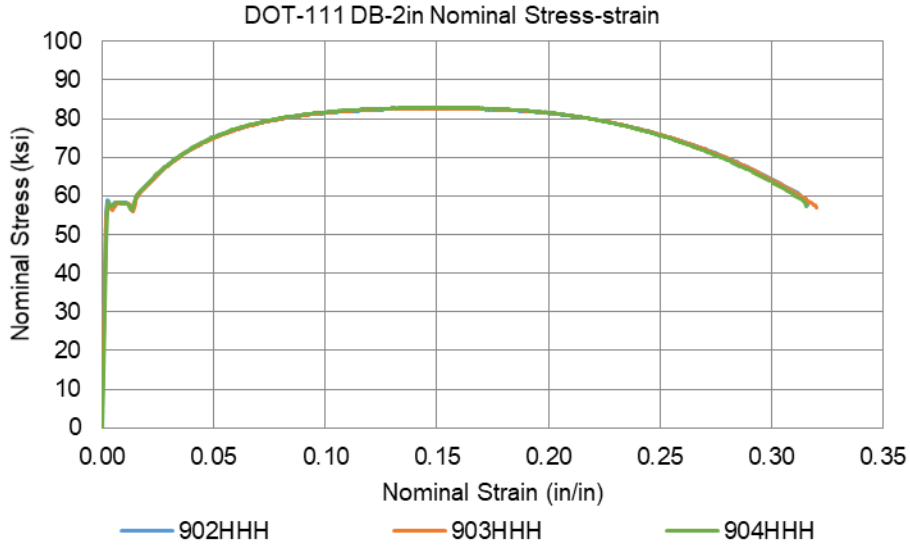

Figure A2. Nominal Stress-Strain Tensile Results from Flat 2-inch Gage Length Coupons (DB-2in) Cut from DOT-111

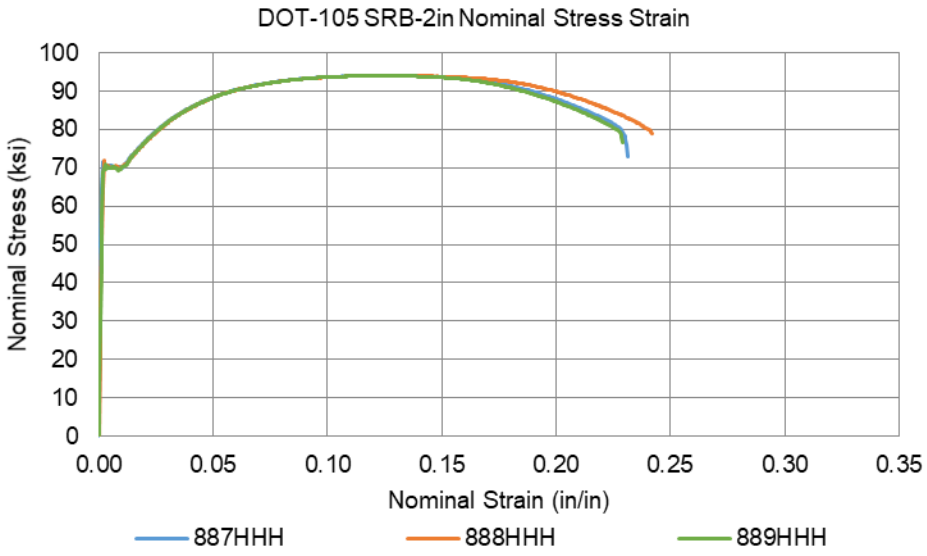

Figure A3. Nominal Stress-Strain Tensile Results from Round 2-inch Gage Length Coupons (SRB-2in) Cut from DOT-105

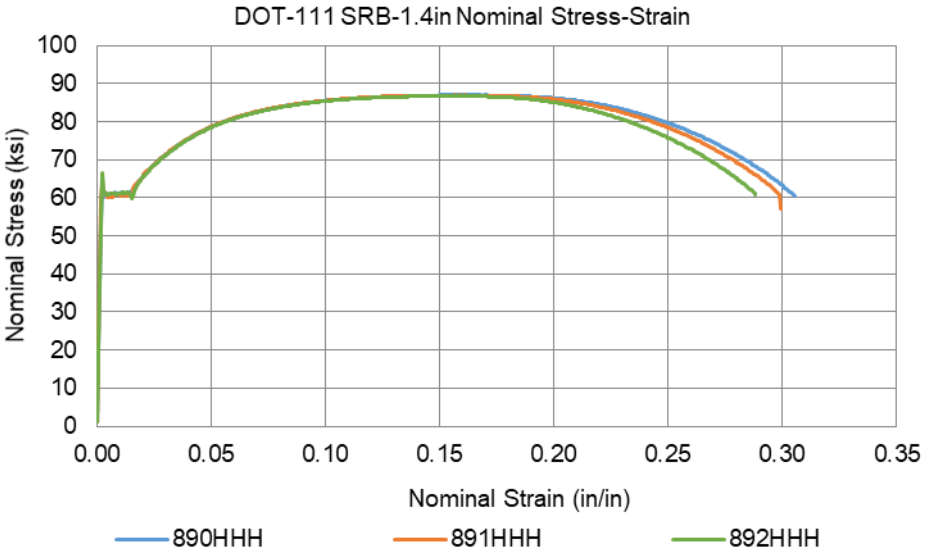

Figure A4. Nominal Stress-Strain Tensile Results from Round 1.4-inch Gage Length Coupons (SRB-1.4in) Cut from DOT-111

Abbreviations and Acronyms

ACRONYMS	EXPLANATION
AAR	Association of American Railroads
ASTM	American Society for Testing and Materials
B-W	Bao-Wierzbicki
DOT	Department of Transportation
DB	Dogbone
EB	Elongation at Break
FRA	Federal Railroad Administration
FE	Finite Element
LSTC	Livermore Software and Technology Corporation
NRB	Notched Round Bars
PEEQ	Plastic Equivalent
PHMSA	Pipeline and Hazardous Materials Safety Administration
RA	Reduction in Area
TC	Transport Canada
SBR	Smooth Round Bar
SwRI	Southwest Research Institute
TRIAX	Stress Triaxiality
TTC	Transportation Technology Center (the site)
TTCI	Transportation Technology Center, Inc. (the company)
UTS	Ultimate Tensile Strength
Volpe	Volpe National Transportation Systems Center
YS	Yield Strength